

Effects of Edge-Seal Design on the Mechanical and Thermal Performance of Vacuum-Insulated Glazing

Wenyuan Zhu^a, Bipin Shah^b, Sarma Gorti^c, Mahabir Bhandari^d, Adrian S. Sabau^c and Seungha Shin^{a*}

^a *Department of Mechanical, Aerospace, and Biomedical Engineering, University of Tennessee, Knoxville, TN, 37996, USA*

^b *WinBuild, Inc., Fairfax, VA, 22030, USA*

^c *Computational Sciences and Engineering Division, Oak Ridge National Laboratory, Oak Ridge, TN, 37831, USA*

^d *Buildings and Transportation Science Division, Oak Ridge National Laboratory, Oak Ridge, TN, 37831, USA*

* Corresponding author: sshin@utk.edu

Abstract

Although vacuum-insulated glazing (VIG) has been proposed as a promising solution towards developing energy-efficient buildings, VIGs have not become popular in the market due to several technical challenges including the complexity of the fabrication process. In particular, the edge-seal is a key component that significantly affects the thermal insulation and mechanical performance, and the development of edge-seal with adequate thermal insulation, mechanical strength, and reasonable processing cost is essential to overcome such technical issues in VIG. For this purpose, effects of edge-seal design parameters on the VIG performance should be identified. In this research, we analyzed the edge-seal for thermal transport as well as structural stresses to study the effects, and then identified and evaluated the material mixes for the edge-seal requirements. The finite element simulations showed the significance of VIG corner calculation on overall thermal transmittance and the importance of seal conductivity below 1 W/m.K. The experiments with the flexible seals with different ratios of fine glass powder demonstrated that the measured shear strength values for the seal with less than 30% glass powder were more than 10 times larger than the calculated shear stress values. Based on these simulation and experimental results, a flexible sealant was developed using a proprietary mix of ceramic materials that meets the requirements of the designed VIG edge-seal, including structural as well as thermal stress resistance and a low conductivity. Moreover, the sealant is self-curing under atmospheric conditions, and thus it does not require costly inline process of laser curing or oven baking.

Keywords: edge-seal design; vacuum-insulated glazing; thermal insulation; mechanical performance; flexible sealant.

This manuscript has been authored by UT-Battelle, LLC, under contract DE-AC05-00OR22725 with the US Department of Energy (DOE). The US government retains and the publisher, by accepting the article for publication, acknowledges that the US government retains a nonexclusive, paid-up, irrevocable, worldwide license to publish or reproduce the published form of this manuscript, or allow others to do so, for US government purposes. DOE will provide public access to these results of federally sponsored research in accordance with the DOE Public Access Plan (<http://energy.gov/downloads/doe-public-access-plan>).

Nomenclature

| | |
|-----|---|
| A | area, mm ² |
| C | areal thermal conductance or heat transfer coefficient, W/m ² .K |
| E | elastic modulus, MPa or GPa |
| G | shear modulus, MPa or GPa |
| h | gap (seal or pillar) height, mm |
| k | thermal conductivity, W/m.K |
| P | pressure, N/m ² |
| Q | heat flow, W |
| q | heat flux, W/m ² |
| R | areal thermal resistance, m ² .K/W |
| r | pillar radius, mm |
| U | overall heat transfer coefficient, W/m ² .K |

Greek letters

| | |
|---------------|--------------------|
| ε | emissivity |
| λ | pillar spacing, mm |
| ν | Poisson's ratio |
| τ | shear stress, MPa |

Subscripts

| | |
|-------------|----------------------------------|
| <i>in</i> | indoor |
| <i>out</i> | outdoor |
| <i>max</i> | maximum |
| <i>seal</i> | sealant |
| <i>pa</i> | pillar |
| <i>EPDM</i> | ethylene propylene diene monomer |
| <i>rad</i> | radiation |
| <i>vac</i> | vacuum |

1 Introduction

Conventional windows used in most buildings are comprised of glass panes that are separated by air or inert gas to limit the heat transfer between them. Vacuum-insulated glazing (VIG) offers the promise of superior performance by taking advantage of vacuum to limit the conduction and convection between the layers of glass.^[1] Even though windows occupy between 10-15% of the total envelop area of a home which is exposed interacts with outside environment, they account up to 30% of the heat loss ^[2], i.e., windows are responsible for more than five to six times of energy loss, compared to walls. Therefore, the development of improved insulating glass units, such as VIG, has gained significance in recent years ^[3-5], and the building retrofitting including the application of VIG can effectively contribute to the reduction of greenhouse gas emission.^[6] VIG is an assembly of two or more glass panes separated by pillars and hermetically sealed along the periphery to maintain the vacuum in the gap between the glass panes.^[7] For more effective thermal insulation or higher thermal resistance (*R*-value), air needs to be evacuated to a level that prevents convection in the cavity, typically lower than 10^{-3} Torr (0.133 N/m^2) ^[8]. VIG, if successfully deployed in the market, will be a promising replacement of single pane glazing which can minimize heat loss while maintaining visibility and daylighting.

Windows in which VIG is installed are exposed to harsh environmental conditions, e.g., wind pressure, rainwater, and temperature fluctuations. For VIG to be thermally insulating ^[9,10] and durable ^[11,12], the optimized design of the gap region, including edge-seal, support pillar array, and vacuum is important as the thermal resistance of the gap region is dominant in the overall heat transfer. Various design parameters of the support pillars have been intensively studied, demonstrating their effects on thermal and mechanical performance of VIG ^[13-16]. In addition to the study of pillar materials and geometry, the location of the low emissivity coating has also received attention ^[17,18]. On par with the significance of the support pillar design shown in these previous studies, the edge-seal design is also expected to be critical to the VIG performance, and material and design parameters of the edge-seal need to be comprehensively investigated for their optimal design. Exposure to the harsh environmental conditions also makes it critical to implement an edge-

seal design that will be able to withstand such conditions. Failure of the edge-seal would reduce the thermal resistance of the VIG from R-10 (U -value of $0.1 \text{ W/m}^2\cdot\text{K}$) to R-3 (U -value of $0.33 \text{ W/m}^2\cdot\text{K}$), which substantially degrades the thermal insulation of windows.

Along with the pillar design, the edge-seal design plays a significant role in controlling the thermal transport and providing stress resistance, and therefore, improving the seal design can help enhance the thermal and mechanical performance of the VIG. Research has shown that nearly 50% of the overall heat transfer occurs through the edge-seal part ^[19], and depending on its design parameters, this ratio can be even larger. Therefore, the goal of the effort described in this paper is to understand the correlation between edge-seal design and VIG performance, particularly in terms of the seal material parameters, which would be beneficial to improve the thermal and mechanical performance of VIG.

Since 1980, investigations of how edge-seal materials affect the performance of regular windows and evacuated windows were carried out by many researchers ^[19-23]. In these studies, the focus was mainly on choosing a material to improve both mechanical and thermal performance of VIG using experimental tests. However, the experimental method has undesirable disadvantages in terms of the high cost and low efficiency, and each test requires preparation of several different materials and fabrication of many VIG samples. Another drawback is the difficulty in testing the effect of changes in the seal geometry in the VIG sample, which requires a redesign of the sample each time.

To overcome these disadvantages, computational methods have been applied to complement the experimental studies, which allowed for changes to the material properties and geometry to be evaluated much more quickly and efficiently through simulations. Since the 2000s, researchers began to study the edge-seal effect using computational methods ^[20]. For example, by investigating the effect of seal size with the finite element method (FEM), the research found that reducing the width of the seal could lead to a thermal transfer reduction of around 20% ^[13]; an alloy-seal was evaluated using both experiment and FEM to determine its advantage and disadvantage for sealing application ^[21]; and the effect of different seal layers

mixed with metal wire on the VIG performance was investigated using experimental and computational methods [22,23].

The previous efforts related to the study of edge-seal effect have focused on specific materials for the edge-seal, and mainly on the thermal performance of the VIG. In this work, for the first time, the effects of several edge-seal material parameters on both the mechanical strength and the thermal insulation of VIG were examined using 3D finite element method (FEM) simulations and experiments. FEM simulations were used to guide the selection of the required material parameters for the desired thermal and mechanical response of the VIG. An important contribution of the work presented here is that the performance of several flexible seals was evaluated experimentally, which differs from the more rigid seal materials used in earlier studies, with the consequence of shear stress reduction due to the low modulus of the flexible seals. This study is organized as follows. In Section 2.1, the computational methodology including the generic VIG geometry, the material properties, and the simulation conditions is presented. The experimental methodology for the fabrication and mechanical testing of flexible seal mixes is described in Section 2.2. In Section 3.1, simulation results of the VIG thermal performance are presented with discussions on the effects of various edge-seal parameters. In Section 3.2, the results of experimentally measured mechanical strength and sealing tightness are presented for flexible seal mixes, and in Section 3.3, numerical thermo-mechanical simulation results are presented for several values of the seal elastic modulus. Based on the combined experimental and simulation analyses, a flexible seal material has been developed, which satisfies the desired thermal and mechanical performance requirements of the VIG.

2 Methodology

2.1 Computational Approach

Simulations were carried out in this work using the finite element method to examine how edge-seal design and material properties affect the thermal and mechanical performance of the VIG. The modeled VIG consists of two panes of glass separated by an array of regularly spaced pillars, which prevent the glass

panes from collapsing into each other when vacuum is introduced in the gap between them (Fig. 1). The vacuum is maintained by two layers of sealant material around the edges of the VIG. The top and bottom glass panes of the modeled VIG were assumed to be exposed to the outdoor and indoor environment, respectively. The dimensions of each glass pane were taken to be $(1,000 \times 1,000 \times 3) \text{ mm}^3$, and the top glass pane was assumed to have a low-emittance coating (emissivity $\varepsilon = 0.018$) on its inner surface. The pressure of the gap (P_{vac}) was set to 10^{-3} Torr (0.133 N/m^2), which is very similar to the vacuum pressure value in conventional VIG products.

A baseline configuration of the VIG unit was considered for the study of edge-seal effects, and it consisted of cylindrical pillars with a height of $h = 1 \text{ mm}$ and radius of $r = 0.5 \text{ mm}$ placed in the gap between the two glass panes. The pillars were arranged in the form of a square array with a pillar spacing (λ) of 50 mm . At the outer edges of the glass panes, the thickness and width of a primary seal were 1.4 mm and 5 mm , respectively, and those of a secondary seal were 1 mm and 7.5 mm , respectively. The primary seal thickness is more than the secondary seal thickness to accommodate the groove which prevents vacuum loss. The secondary seal is used to limit shear stress due to thermal expansion of the outer pane of glass exposed to extreme weather and to ensure vacuum retention for longer period. To simulate the installation of the VIG within a window frame, ethylene propylene diene monomer (EPDM) rubber with thermal conductivity $k_{\text{EPDM}} = 0.25 \text{ W/m.K}$ was included on the surfaces of both glass panes along the outside edge to span the width of the primary and secondary seals of the VIG (12.5 mm). Material properties employed in the FEM model are summarized in Table 1. It should be noted that the elastic modulus and thermal conductivity listed for the primary seal are nominal values, and these parameters were varied to study their effect on the VIG performance. The pillar thermal conductivity listed below corresponds to a ceramic composite material, and has a thermal conductivity similar to that of glass. The pillar thermal conductivity was also varied in some of the simulations discussed later.

Because of the symmetry of the modeled VIG, a quarter section $(500 \times 500 \times 3) \text{ mm}^3$ of the full unit was used in this work, which includes all the different components, including the primary and secondary seals

and the EPDM. A schematic of the quarter VIG unit is shown below (Fig. 1), along with the arrangement of the seals, where the primary seal is in contact with the vacuum gap while the secondary seal is in contact with the outside air. The two seals are joined to each other, and are perfectly bonded to the top and bottom glass panes, which serves to ensure that there is no loss of vacuum from the gap between the glass panes.

Table 1. Material properties of VIG components used in the finite element simulations of this study

| Component | Density (g/cm³) | Elastic modulus <i>E</i> (GPa) | Poisson's ratio ν | Specific heat (J/kg.K) | Thermal expansion coefficient ($\times 10^{-6}$ K⁻¹) | Thermal Conductivity <i>k</i> (W/m.K) |
|-----------------------|---------------------------------------|---|---|---------------------------------------|---|--|
| Glass | 2.5 | 73 | 0.22 | 800 | 8.6 | 1 |
| Pillar | 3.5 | 280 | 0.22 | 800 | 8.6 | 1 |
| Primary seal | 2.5 | 75 | 0.22 | 800 | 20 | 1 |
| Secondary seal | 1.54 | 3.5 | 0.33 | 1,000 | 50 | 0.136 |
| EPDM | 1.4 | 2.5 | 0.47 | 1,000 | 80 | 0.25 |

The FEM simulations were used to investigate the effect of changing the thermal and mechanical properties of various components on the response of the VIG. Through mesh-convergence tests,^[15] we identified optimal meshing conditions for the accuracy and computational efficiency of the FEM simulations, where all the element sizes were smaller than 10^{-4} mm³. Parameters that were varied in the study include the thermal conductivity of the primary seal and the pillars, the width of the primary seal, and the elastic modulus of the primary seal. Effects of changing these parameters on the overall heat transfer coefficient (*U*-value), the heat flux distribution, and the stress distribution in the VIG unit were examined. The commercial program ABAQUS ^[24] was used to carry out all of the FEM simulations for thermal and mechanical analysis.

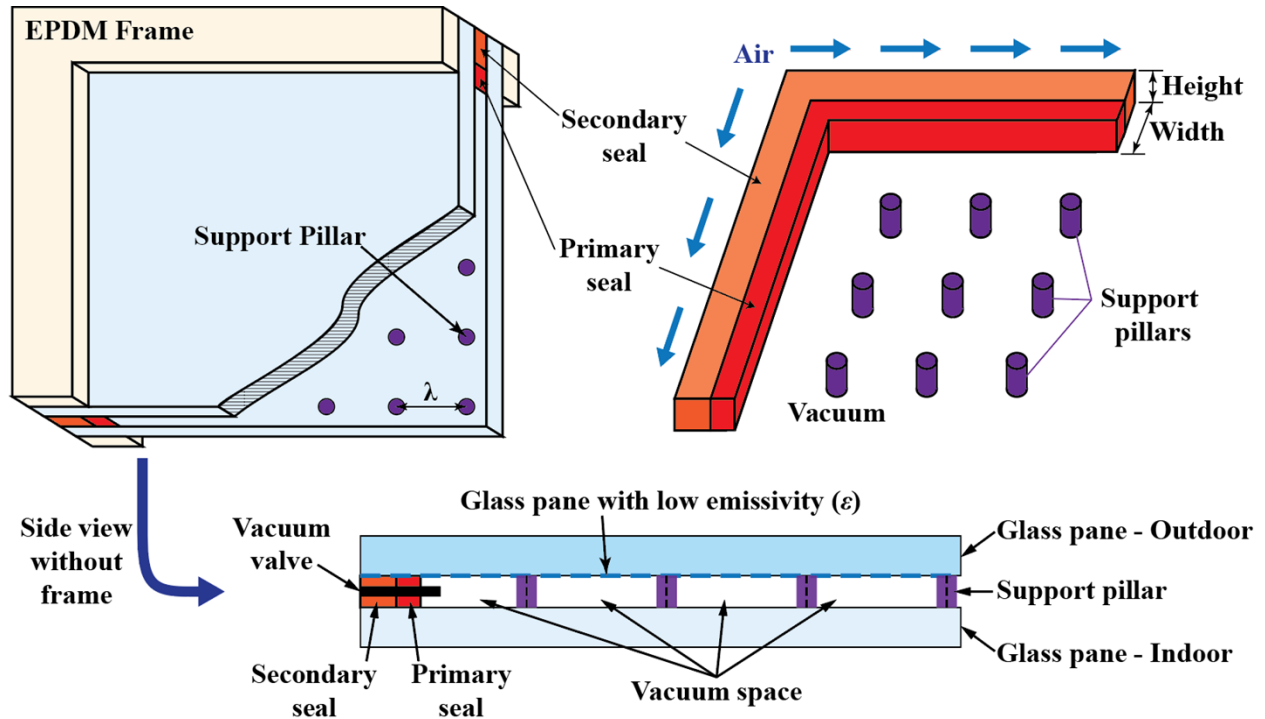


Figure 1. A quarter-section model of the VIG unit showing the location of various components.

Thermo-mechanical analyses of the VIG unit were carried out to determine the displacement and stress fields in the various components under combined thermal and mechanical loads. A pressure load of $1.01 \times 10^5 \text{ N/m}^2$ (1 atm) was applied to each glass pane on its outer surface, and the gap pressure between the glass panes was assumed to be 10^{-3} Torr (0.133 N/m^2). Symmetry boundary conditions along the x and y directions were employed for the two sides of the model corresponding to the centerline of the full VIG, while the top and bottom surfaces of the EPDM frame were restrained to have no displacement, as shown in Fig. 2. Interaction between the top glass pane and each pillar was modeled assuming frictionless contact, while a cohesive interface condition with a stiffness value of 10^3 N/mm^3 was employed between the bottom glass pane and each pillar. In order to simulate two extremes for the weather conditions, cases with 60°C and -30°C were considered for the outdoor temperatures, while 23°C were used for the indoor temperature, for each case in accordance with ASTM E2188 [25] and E2190 [26] durability test conditions. Heat transfer coefficients over the outer surfaces of the top (outdoor, C_{out}) and bottom (indoor, C_{in}) glass panes were $8 \text{ W/m}^2\cdot\text{K}$ for the thermo-mechanical simulations. The emissivity value of 0.84 were used for all glass surfaces except the inner surface of the top outdoor glass whose emissivity was assumed to be 0.018 to

model a low-emittance coating.

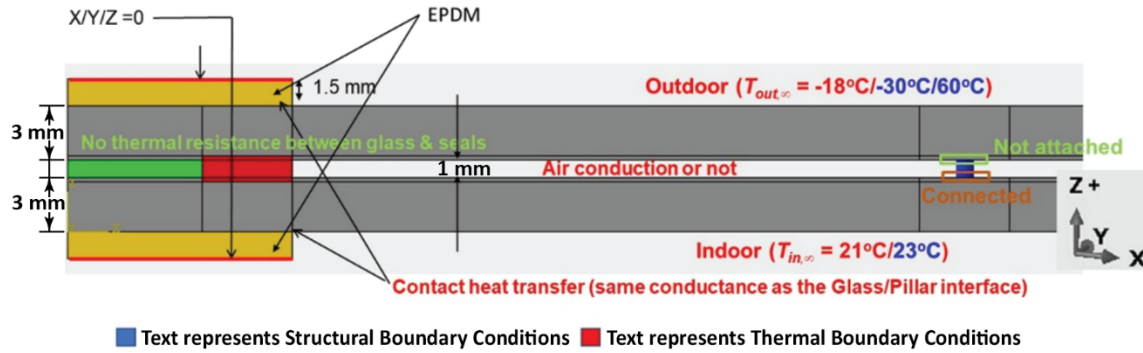


Figure 2. Modeling specification for thermal and structural analysis.

In addition to the thermo-mechanical analysis described above, simulations involving only thermal analysis were carried out to study the thermal insulation of the VIG, which is evaluated by examining U -value, i.e., the overall heat transfer coefficient. These simulations assumed steady-state conditions, with a standard temperature condition of -18°C for outdoor air and 21°C for indoor air. 29.41 and 6.67 $\text{W}/\text{m}^2\cdot\text{K}$ were employed as heat transfer coefficients on outer surfaces of the top outdoor and bottom indoor glass panes (C_{out} and C_{in}), respectively, and the emissivity values at the inside surfaces of the glass panes were the same as those described above. These boundary conditions were based on guidelines in the ASTM C1199 [27] testing procedure. It was assumed that the pillars and seal were in perfect contact with the glass surfaces, leading to zero thermal resistance at these interfaces. Because of the symmetry, adiabatic boundary conditions were applied along the sides normal to the x and y axes. The overall heat transfer coefficient or U -value was calculated as

$$U = Q / (A_{eff} \Delta T), \quad (1)$$

where Q is the total heat transfer rate across the glass panes from one side to the other of the VIG model, A_{eff} is the effective in-plane area for the VIG model (using the area of the model when viewed from the top/bottom), and ΔT is the difference in temperature between outdoor and indoor environments. Q is evaluated by integrating the heat flux from the FEM simulation output over the effective surface area ($Q = \sum q_i A_i$). Table 2 provides details of the VIG configuration used for the benchmark simulations.

Table 2. VIG configuration and properties for baseline simulations

| Parameter | Value |
|---|---------------------------|
| VIG glass dimension (width × height) (mm ²) | 1,000 × 1,000 |
| Glass pane thickness (mm) | 3 |
| Emissivity/Low emissivity coating | 0.84/0.018 |
| Vacuum gap or pillar height (mm) | 1 |
| Pillar radius (mm) | 0.5 |
| Pillar spacing (mm) | 50 |
| Pillar thermal conductivity (W/m.K) | 1 |
| Primary seal (width × height) (mm ²) | 5 × 1.4 |
| Secondary seal (width × height) (mm ²) | 7 × 1 |
| Thermal conductance of vacuum (W/m ² .K) | 1.0679 × 10 ⁻³ |

2.2 Experiment

Fabrication of Flexible Seals and Samples

Various flexible seals were prepared by adding different amounts of glass powder to a proprietary flexible ceramic seal, considering their eventual application as both primary and secondary seals. The powder grain size was less than 0.2 mm, and the volume fraction of the added glass powder in the flexible seal mix ranged from 0 to 50%. Addition of glass powder increases the viscosity and reduces the fluidity of the sealant, as Fig. 3 shows. Also, greater resistance to gas permeability was expected from the glass powder addition.

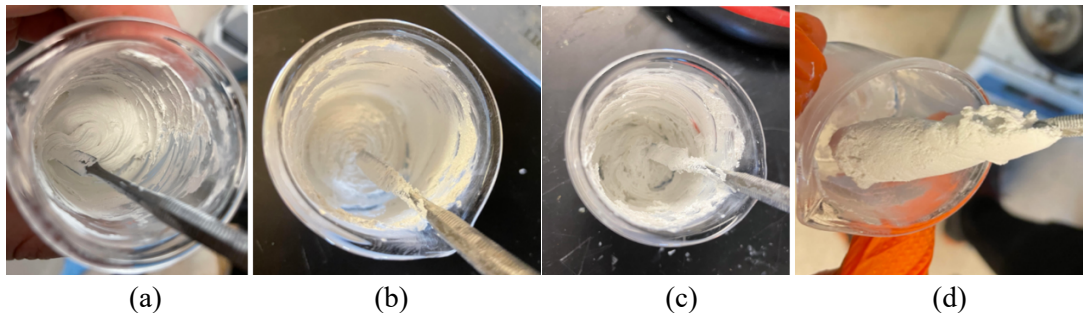


Figure 3. Flexible seal mix with different volume ratios of glass powder smaller than 0.2 mm. The volume fraction of (a) 10% glass powder; (b) 30% glass powder; (c) 40% glass powder; and (d) 50% glass powder.

Using the prepared flexible seal mix, three types of samples were fabricated to evaluate the performance of the glass seal. For the first type of sample, two 38.1 mm × 76.2 mm (1.5" × 3") glass panes with thickness

of 3 mm were aligned with a 5 mm shift and bonded by applying a single line of flexible seal mix. The gap between the glass panes was maintained by four glass pillars with 1 mm height, and the applied seal width is 5 mm, as shown in Fig. 4a. This type of sample was mainly used in the shear strength test. To test the effectiveness of the sealing of two glass panes, we employed two square glass panes of size 76.2 mm \times 76.2 mm (3" \times 3") and applied the flexible seal on the peripheral region with 5 mm width, as shown in Fig. 4b. Lastly, for the VIG demonstration, sealing of two 152.4 mm \times 152.4 mm (6" \times 6") glass panes was achieved, including nine glass pillars and the flexible seal, along with the installation of a vacuum valve (Fig. 4c).

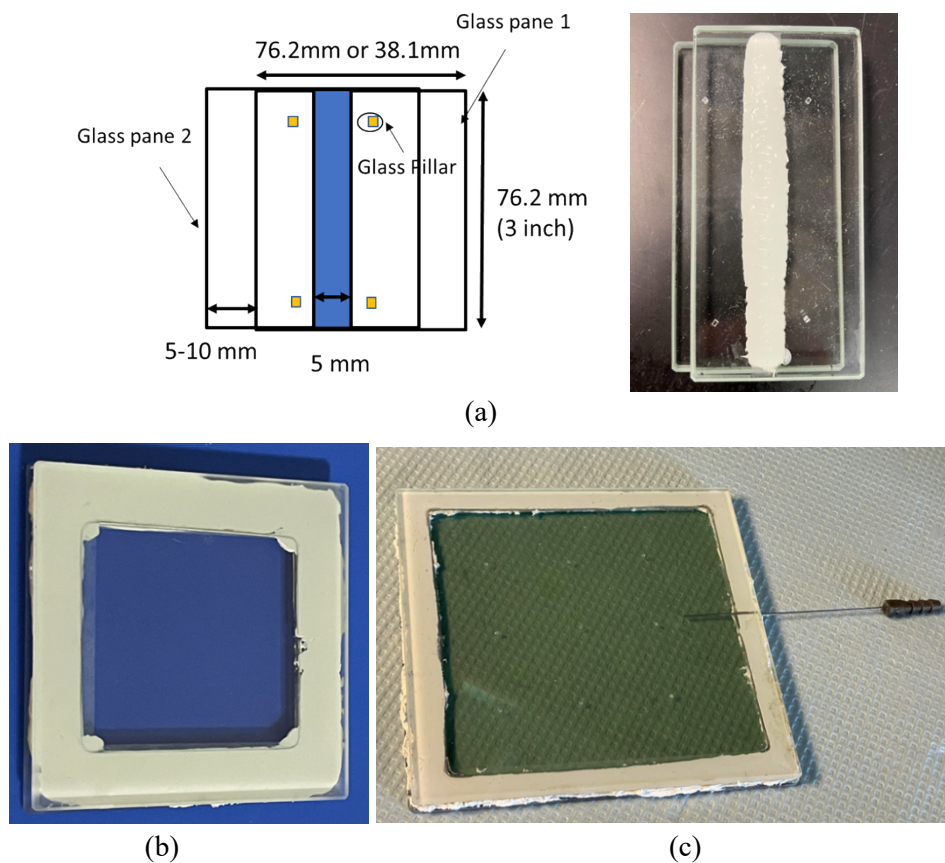


Figure 4. Three different samples for experimental tests (a) 38.1 mm \times 76.2 mm (1.5" \times 3") glass with single line flexible seal, mainly used in shear stress test, (b) 76.2 mm \times 76.2 mm (3" \times 3") glass with flexible seal, and (c) 152.4 mm \times 152.4 mm (6" \times 6") glass with flexible seal.

The vacuum valve (patent pending) is placed in the plane of the glass pane, and then the edge sealant is applied, following which the second glass pane is positioned, and the assembly is formed by applying pressure and allowing it to dry. Upon drying, vacuum is drawn from the VIG using a conventional high

vacuum pump, and once the desired vacuum (pressure level $\leq 10^{-3}$ Torr) is achieved, the vacuum valve is welded and then the pump is detached. This allows the vacuum to be retained in the VIG. This process was tested to confirm vacuum retention and prevention of leaks. Vacuum level of 10^{-3} Torr (0.133 N/m^2) was kept in place for 6 days to confirm retention, followed by helium test to ensure that there were no leaks. In all three cases, the sealant between the two glass panes was cured for 24-48 hours at room temperature for the vulcanization of the sealant.

Seal Evaluation

To assess the mechanical performance and product reliability of VIG, airtightness and maximum shear strength were measured. Immersion in a water container and placement of the sample in a freezer were used for determining the airtightness, while a tensile testing machine was used for the shear stress test, as shown in Fig. 5a.

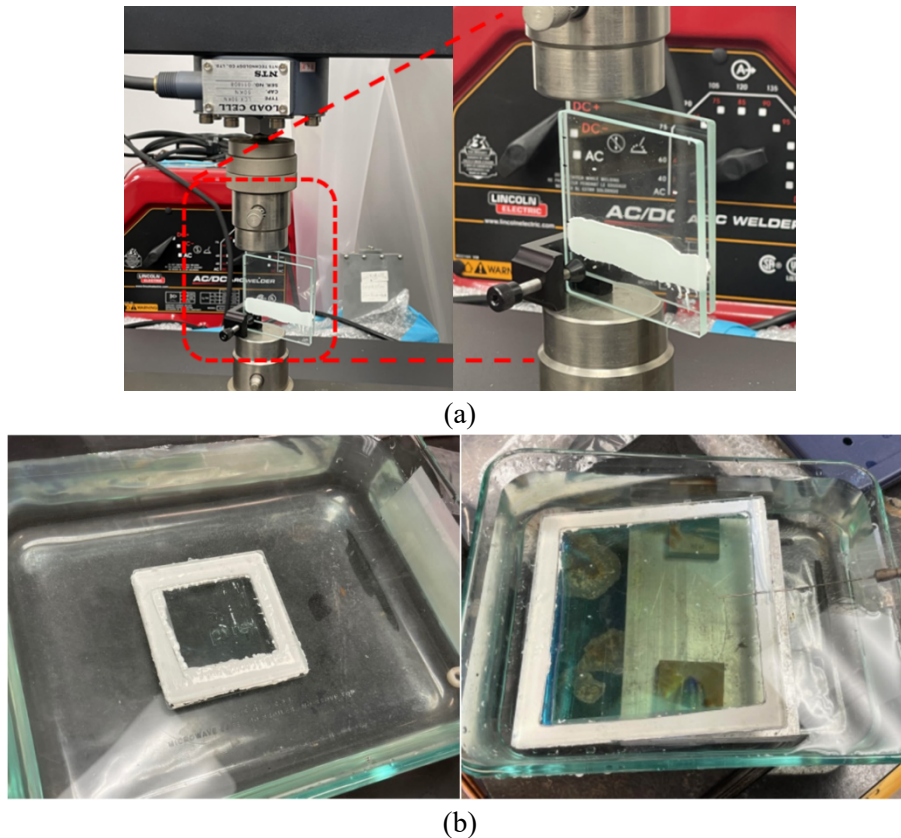


Figure 5. (a) Tensile testing machine (Model QC-TECH B5000) with a sample inside, and (b) Water leakage test.

To guarantee its efficiency in fabrication and accuracy in the test, type 1 samples with a smaller dimension of glass and controlled single line of seal were employed for the shear strength measurement. After a shear-lap sample was vertically aligned and clamped in a tensile testing machine (Model QC-TECH B5000 system), increasing compressive force was applied until the seal was broken. The force and glass displacement were recorded, and using the recorded data along with the seal geometry, stress-strain curve was plotted for the measurement of the seal shear strength. Additionally, type 2 samples with flexible seal mix were used for the water leakage test to ensure its sealing performance. The samples were dipped into water of 9 mm depth for 48 hours, and then checked to see if any water leakage or water vapor is observed, as shown in Fig. 5b. Thermal conductivity of the edge seal material was determined by preparing and testing a 100 mm by 100 mm sample using ASTM C518 test procedure [28]. The test results obtained are presented in Table 3 and showed that the conductivity of the flexible edge sealant was 0.136 W/m.K.

Table 3. Thermal conductivity measurement of the flexible edge seal

| Test # ASTM C518 | Specimen | Thickness, mm | Temperature (External HFTs), °C | | Thermal Conductivity (External HFTs), W/m.K | | |
|---------------------|---------------------------|------------------|------------------------------------|-------|--|-------|---------|
| | | | Upper | Lower | Upper | Lower | Average |
| 694 | Edge Seal Flex Sealant | 8.13 | 16.6 | 31.6 | 0.148 | 0.125 | 0.136 |

3 Results and Discussion

In a recent paper [15], the computational approach using ABAQUS described earlier has been validated by comparing the computed center-of-glass U -value against experimental measurements on a VIG sample, as well as against a simple one-dimensional analytical calculation. The analyses described in this paper have been carried out using this validated FEM model.

3.1 Effect of Seal Parameters on the Thermal Response

As mentioned earlier, while the pillar array between the glass panes serves as the main conduit for heat transfer in the region near the VIG unit center, the regions near the edges comprised of the primary and secondary seals and the frame account for a significant fraction of the overall heat flux across the VIG unit. A comparison of the U -values computed for the full VIG unit with those from a unit cell model that excludes the edge effects showed that there is a substantial increase in the U -value for the full VIG [15]. This change in U -value is dependent on the properties of the primary and secondary seal materials. Therefore, it is important to understand the effects of these seal properties on the overall response of the VIG unit.

Effect of Primary Seal Thermal Conductivity

The effect of the primary seal thermal conductivity on the overall heat transfer across the VIG unit was investigated using the FEM simulations. Figure 6 shows the variation of the U -value of the full VIG with respect to the seal thermal conductivity, k_{seal} . For each value of k_{seal} , the variation of the U -value was also examined for different pillar thermal conductivity values, k_{pa} . To clearly identify the influence of k_{pa} , the pillar conductivity was varied up to 999 W/m.K, considering it as an extreme case. The results in Fig. 6 show that for a given value of k_{pa} , the U -value increases with k_{seal} , with the rate of increase being quite high at low k_{seal} , and the U -value curve flattening out at higher values of k_{seal} . The overall shape of the U -value curve is the same for different k_{pa} values, except for a shift to higher U -values with increase in k_{pa} . This shift is much greater at low k_{pa} values, but becomes considerably smaller beyond about $k_{pa} = 16$ W/m.K. Thus, the following thermal simulations discussed later also employed $k_{pa} = 16$ W/m.K as one extreme (close to thermal conductivity of stainless steel) in addition to 1 W/m.K listed in Table 2.

It can be deduced from the above results that for a given pillar thermal conductivity, the thermal influence due to the seal diminishes at higher values of the seal thermal conductivity and reaches a plateau for values of k_{seal} larger than 1 W/m.K. If we consider flexible seal materials, most of them have a thermal conductivity value below 1 W/m.K [29], and therefore, it is necessary to consider their effect on the overall VIG thermal performance.

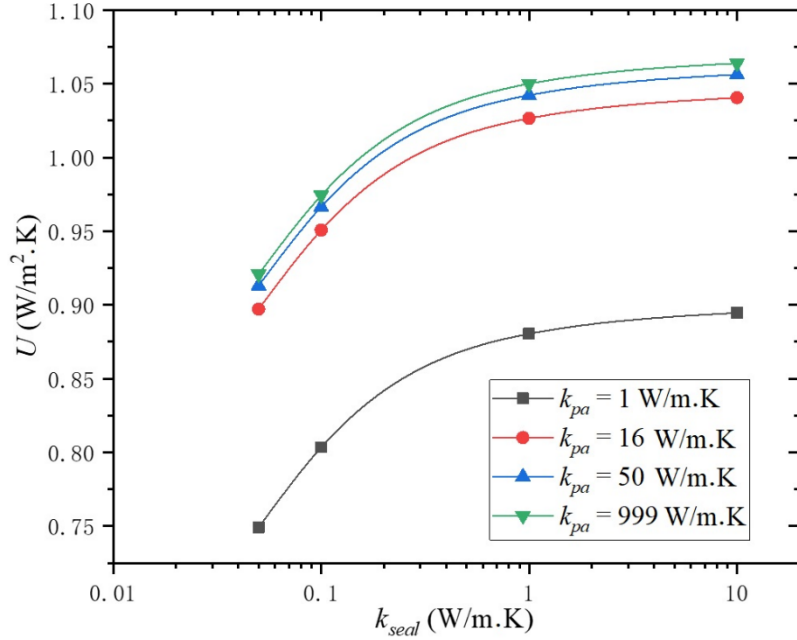


Figure 6. U -value of the full VIG for different thermal conductivities of seal and pillar, with k_{seal} varying from 0.05 W/m.K to 10 W/m.K, and k_{pa} varying from 1 W/m.K to 999 W/m.K.

Heat Flux Distribution

In order to study the seal thermal effect in greater detail, the heat flux (HFL) distribution from the edge to the center of the VIG was examined. We chose two different paths close to one of the symmetry planes of the VIG. While path 1 at the symmetry plane on the top surface of the outdoor glass pane goes through the xy locations of the center of the support pillars, path 2 is shifted by a distance of $\lambda/2$ relative to path 1, so that it does not go through any of the support pillars. The schematic illustration of the two paths is shown in Fig. 7a, and the results of heat flux distribution are presented in Figs. 7b and 7c.

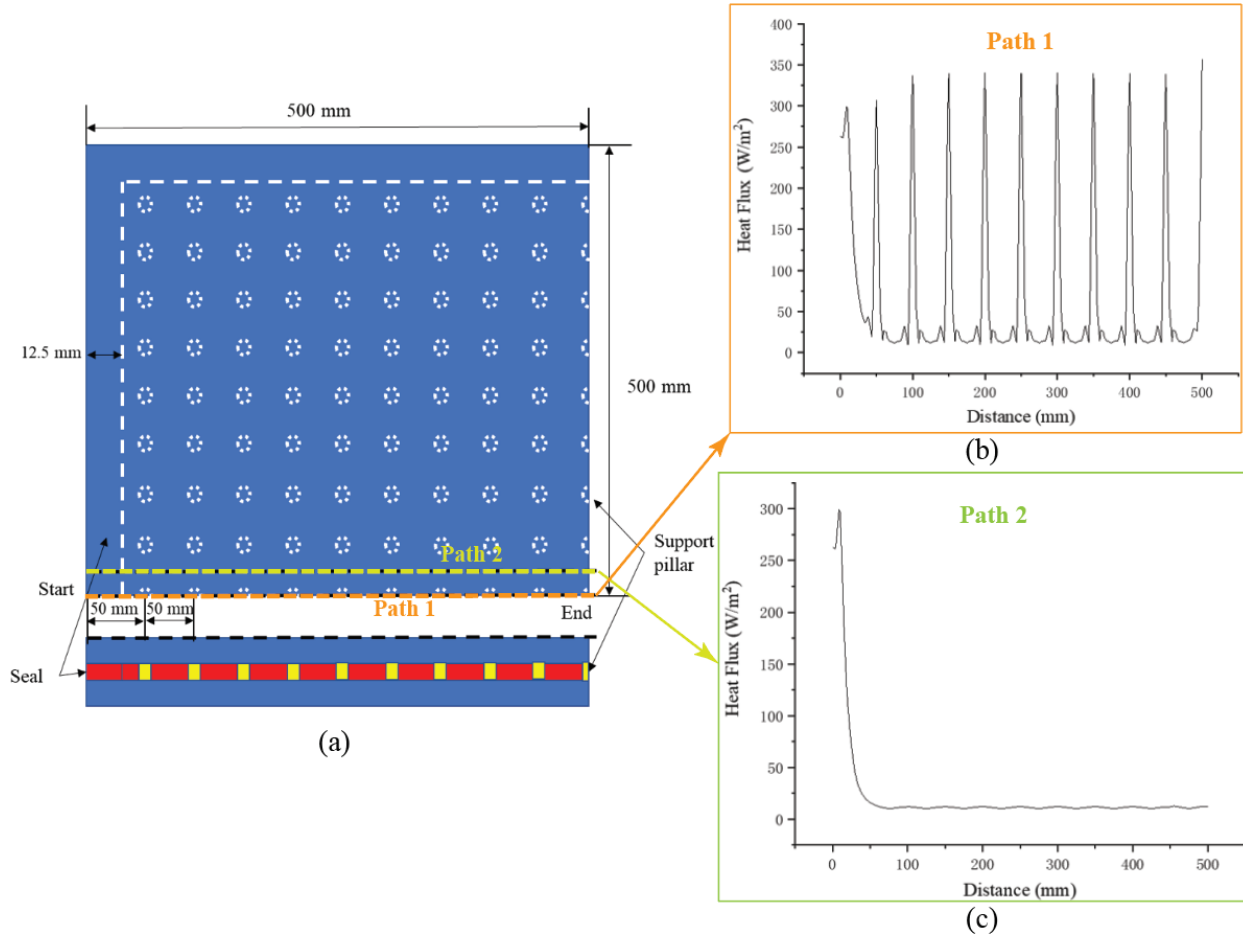


Figure 7. (a) Schematic of VIG FEM model showing two different paths, with path 1 along the center of the VIG, and path 2 shifted by 25 mm ($\lambda/2$) from path 1. (b) Heat flux distribution along path 1 and (c) that along path 2 with $k_{seal} = 1$ W/m.K and $k_{pa} = 16$ W/m.K.

Based on the results, it is observed that the heat flux variations along the two paths show considerable differences. Along path 1, which includes the effect of the pillars, there are local peaks in the heat flux at the locations corresponding to each pillar, whereas the heat flux distribution along path 2 shows minimal effect due to the pillars. After the initial decrease in the heat flux past the edge region, the heat flux distribution becomes more dependent on the pillar properties, and beyond about 100 mm, the effect of the edge section becomes negligible. Therefore, to better understand how the thermal conductivity values of the seal and of the pillar affect the heat flux distribution, we chose a 0-100 mm section of path 1 and path 2 as the new test range to study the influence of different values of k_{pa} and k_{seal} . The results are shown in Fig. 8.

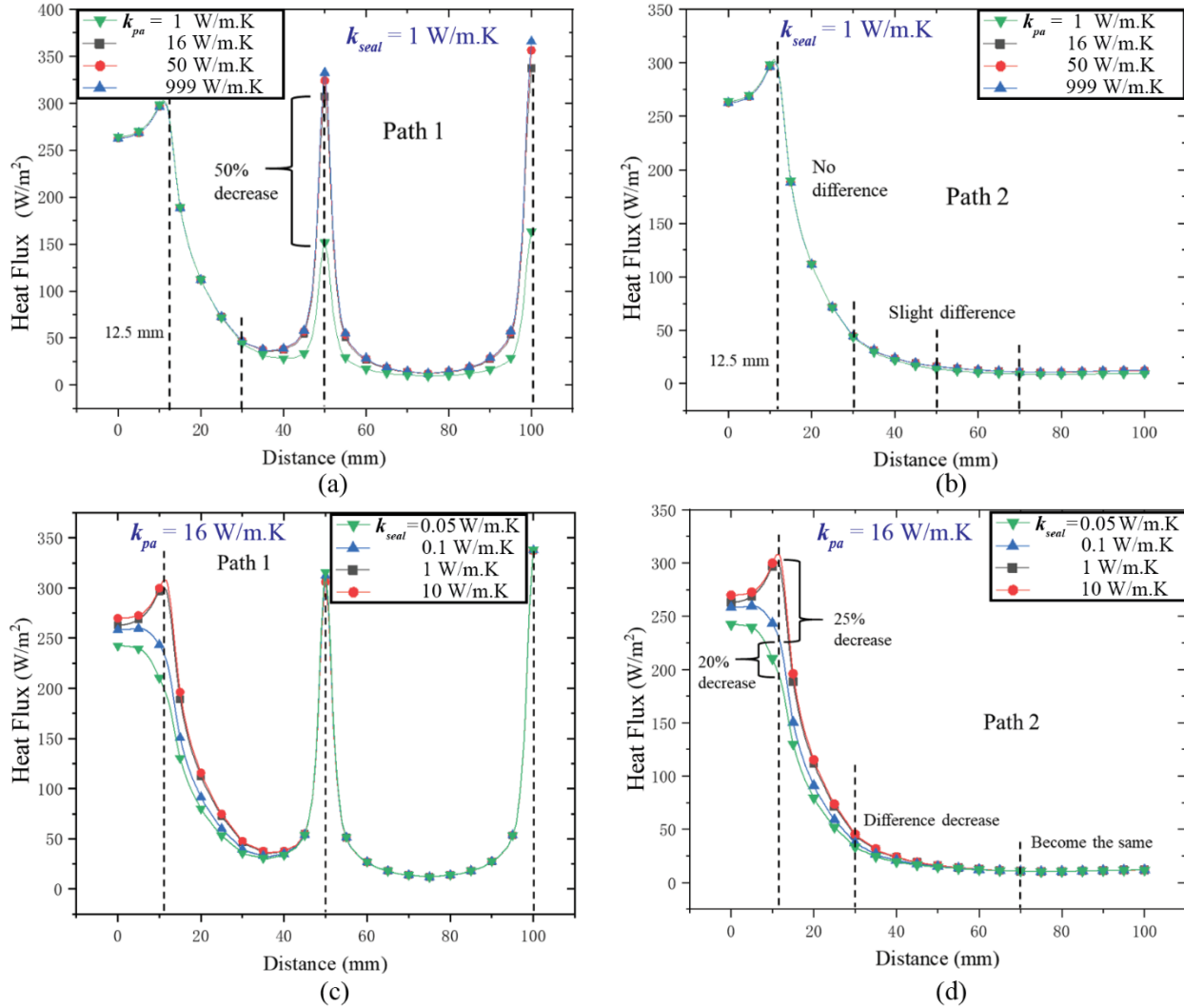


Figure 8. Heat flux distribution along two different paths for different k_{seal} and k_{pa} : (a) heat flux distribution along path 1 with $k_{seal} = 1$ W/m.K and $k_{pa} = 1-999$ W/m.K; (b) heat flux distribution along path 2 with $k_{seal} = 1$ W/m.K and $k_{pa} = 1-999$ W/m.K; (c) heat flux distribution along path 1 with $k_{seal} = 0.05-10$ W/m.K and $k_{pa} = 16$ W/m.K; (d) heat flux distribution along path 2 with $k_{seal} = 0.05-10$ W/m.K and $k_{pa} = 16$ W/m.K.

We calculated the heat flux distribution for different values of the pillar thermal conductivity k_{pa} (1-999 W/m.K) along a portion of path 1 (0-100 mm) and path 2 (0-100 mm), with the thermal conductivity of seal kept fixed at $k_{seal} = 1$ W/m.K. From the plots that are shown in Figs. 8a and 8b, the heat flux around the seal has a high value and generally decreases beyond 12.5 mm, which represents the extent of the seal. The pillar thermal conductivity has an effect on the distribution of the heat flux along path 1 when the distance is larger than about 35 mm, which is almost three times longer than the width of the seal. The local peaks in the heat flux at the pillar locations increase with k_{pa} , although this increase becomes much smaller for k_{pa}

larger than 16 W/m.K. Along path 2, the pillar thermal conductivity effect is also observed beyond about 35 mm, although the differences are very minimal for different k_{pa} values.

In Figs. 8c and 8d, we show the heat flux distribution for different seal conductivity values k_{seal} (0.05-10 W/m.K), while the pillar thermal conductivity is fixed at $k_{pa} = 16$ W/m.K. The thermal conductivity of the seal does not have a significant influence beyond about 35 mm, as noted above. Along path 2, when the distance is larger than 35 mm, the heat fluxes for different k_{seal} values show only a slight difference, and this difference disappears beyond 70 mm. For both paths, the maximum heat flux difference is at the edge of the seal, which shows a 25% decrease when k_{seal} is reduced from 1 W/m.K to 0.1 W/m.K, and a 20% decrease when k_{seal} is reduced from 0.1 W/m.K to 0.05 W/m.K.

Edge-seal Size Effect on VIG Thermal Performance

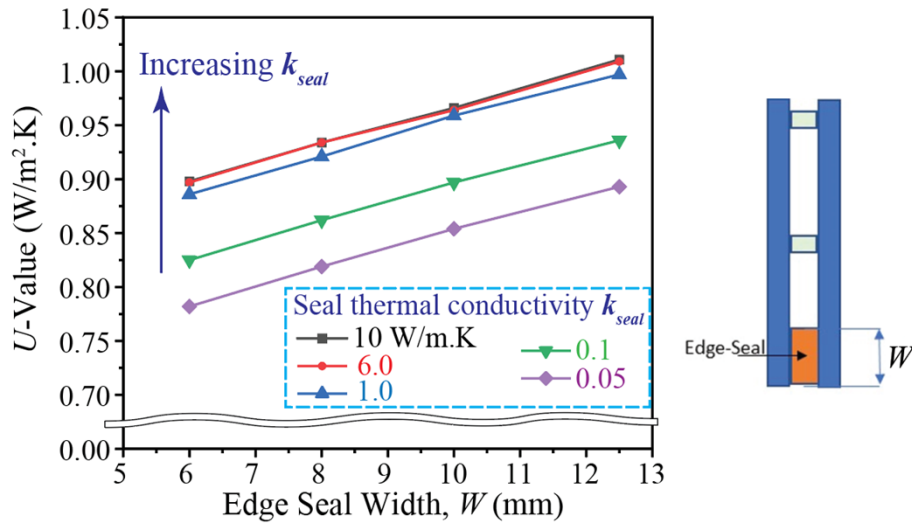


Figure 9. Variation of U -value ($W/m^2.K$) with edge-seal width (W , mm) and thermal conductivity of the seal (k_{seal}).

We also calculated the effect of the edge-seal width, which was varied from 6 – 12.5 mm, on the overall heat transfer coefficient (U -value), for different values of the edge-seal thermal conductivity ranging between 0.05 W/m².K to 10 W/m².K, which are typical values for edge-seal materials available in the market. These calculations were carried out using the WINDOW ^[30] software program mainly for convenience and expediency. The thermal conductivity of the pillars was kept fixed at $k_{pa} = 999$ W/m.K,

and a vacuum of 10^{-3} Torr (0.133 N/m^2) was assumed. From the plots that are shown in Fig. 9 and the data presented in Table 4, the U -value is found to increase with increase in edge-seal width, and the observed difference is $0.11 \text{ W/m}^2\cdot\text{K}$ between 6 mm and 12.5 mm, and this difference is the same for different values of k_{seal} . It is concluded that the edge-seal width in the range of 6 – 12.5 mm does not have a significant impact on the U -value of the VIG unit.

Table 4. U -values computed for different values of edge-seal width and thermal conductivity of the seal

| Seal Width (mm) | U -values ($\text{W/m}^2\cdot\text{K}$) for different k | | | | |
|--|---|-------------|-------------|-------------|-------------|
| | 10 W/m.K | 6 W/m.K | 1 W/m.K | 0.1 W/m.K | 0.05 W/m.K |
| 12.5 | 1.011 | 1.009 | 0.997 | 0.936 | 0.893 |
| 10 | 0.966 | 0.964 | 0.959 | 0.897 | 0.854 |
| 8 | 0.934 | 0.934 | 0.921 | 0.862 | 0.819 |
| 6 | 0.898 | 0.897 | 0.886 | 0.825 | 0.782 |
| Max. U / Min. U | 1.011/0.898 | 1.009/0.897 | 0.997/0.886 | 0.936/0.825 | 0.893/0.782 |
| Max. – Min. | 0.113 | 0.112 | 0.111 | 0.112 | 0.112 |

Corner Effect on VIG Thermal Performance

The windows industry currently uses a two-dimensional (2D) simulation tool (THERM^[31]) to determine the edge-of-glazing thermal transmittance (U -Value). The analysis using THERM was carried out for a cross-section in the middle of the VIG unit, as shown in the schematic in Fig. 9, and the effects of the corner in the full VIG unit are ignored.

In this study, we investigated the impact of the corner on the U -value using the three-dimensional (3D) VIG model. The U -value was calculated using Eq. (1) over a specific region of $100 \text{ mm} \times 100 \text{ mm}$ area at different locations, two of them closer to the middle of the VIG and one at the corner, as shown in Fig. 10a. The temperature difference given by $\Delta T = 21 + 18 = 39^\circ\text{C}$ was considered to compute the U -Value of each zone. The heat flux Q for the area under consideration was obtained directly from the ABAQUS results. It is observed from Fig. 10a that the U -value at the corner (region 1) is considerably higher than at locations away from the corner (regions 2 and 3), indicating that the heat flux is influenced by the location along the periphery of the VIG. This non-uniformity between the corner and the straight edge of the VIG is also

evident from the temperature field of the top glass outer surface shown in Fig. 10b.

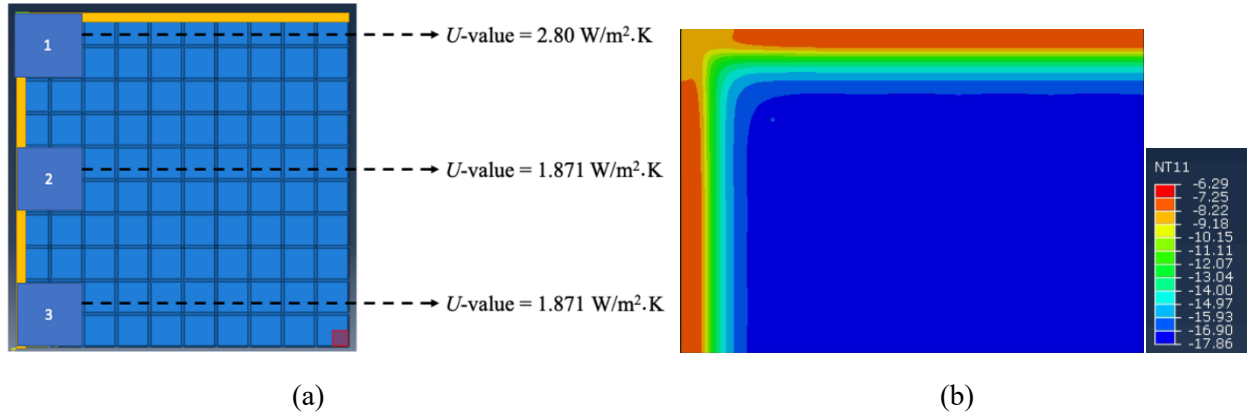


Figure 10. (a) Calculation of U -value over an area of $100 \text{ mm} \times 100 \text{ mm}$ at different locations across the VIG, showing the effect of the corner on the thermal transmittance, and (b) temperature distribution in a section of the top glass pane close to the corner of the VIG unit.

Table 5. Comparison of U -values computed using ABAQUS and WINDOW/THERM (W/T) models for different values of the edge-seal thermal conductivity.

| | U -values ($\text{W}/\text{m}^2\cdot\text{K}$) for different k_{seal} | | | |
|-----------------------|---|--------------------------------------|------------------------------------|-------------------------------------|
| | 0.05 $\text{W}/\text{m}\cdot\text{K}$ | 0.1 $\text{W}/\text{m}\cdot\text{K}$ | 1 $\text{W}/\text{m}\cdot\text{K}$ | 10 $\text{W}/\text{m}\cdot\text{K}$ |
| ABAQUS | 0.921 | 0.974 | 1.050 | 1.064 |
| W/T-100 mm EG | 0.893 | 0.936 | 0.997 | 1.011 |
| W/T-63.5 mm EG | 0.892 | 0.935 | 0.994 | 1.006 |

The importance of including the corner effect becomes evident when the results for the full $1 \text{ m} \times 1 \text{ m}$ VIG unit are examined. A comparison of the U -values calculated using the ABAQUS 3D model with the 2D calculations based on WINDOW/THERM is presented in Table 5. For these calculations, the pillar thermal conductivity was assumed to be $k_{pa} = 999 \text{ W}/\text{m}\cdot\text{K}$, which is the default value in the WINDOW software, and different values of the edge-seal thermal conductivity were considered. It is observed that the 2D results using WINDOW/THERM underpredict the U -Value, while the ABAQUS results lead to a higher U -value due to the inclusion of the corner effect. Even if the edge-of-glass region is taken as 100 mm instead of the currently used 63.5 mm (industry standard), the WINDOW/THERM results show minimal change. It was also observed that as the edge-seal thermal conductivity k_{seal} increases from 0.05 $\text{W}/\text{m}\cdot\text{K}$ to 10 $\text{W}/\text{m}\cdot\text{K}$, the deviation in U -value increases between the 3D and 2D simulation results.

3.2 Experimental Measurement of Mechanical Strength and Sealing Tightness

As the fraction of glass powder increases, the flexible seal mix loses its fluidity before curing. With the ratio larger than 40%, the seal mix does not have sufficient fluidity to make an adequate sealant; therefore, the flexible seal mix with glass powder fractions below 40% (0%, 10%, 20%, and 30%) were tested to investigate the shear strength and airtightness.

All the tested samples of flexible seal mixed with 10-30% ratio of glass powder presented no water leakage or any water vapor after 48 hours of sinking in water, demonstrating an effective sealing performance. No water leakage was observed in the sealing of 152.4 mm × 152.4 mm (6" × 6") glass panes either, which indicated that larger size of glass panes can also achieve the seal airtightness.

The mechanical properties of the flexible seal samples were measured using the shear stress test, where the applied compressive force and the displacement were recorded until the seal was broken (Fig. 11a). As observed in Figs. 11b-11d, increasing the ratio of glass powder in the flexible seal mix results in lower maximum shear stress [= (maximum load)/(seal area); pure flexible seal: 1.18 GPa, seal with 30% of glass powder: 1.17 GPa, and seal with 35% of glass powder: 0.98 GPa]. When the ratio of mixed glass powder increased from 0% to 30%, the maximum shear stress τ_{max} decreased by 1.1%, however, when the ratio of glass powder increased from 30% to 35%, the τ_{max} decreased by 16.5%. That is, up to 30%, the fraction of glass powder does not have a significant effect on the mechanical strength of the seal, while a content larger than 30% deteriorates the strength. Using the measured shear stress and strain, the shear moduli (G) [= (shear stress)/(shear strain) in the linear region] of the flexible seal samples were also evaluated, and then the elastic moduli (E) were estimated [$E = 2G(1 + \nu)$] as 3.71 MPa for the pure flexible seal, 3.78 MPa for the 30% glass powder sample, and 4.29 MPa for the 35% glass powder sample. It is noted that the Poisson's ratio ν was assumed to be 0.5 for the elastic modulus estimation, which is a conservative assumption, and a lower Poisson's ratio value would result in even lower elastic moduli than shown in Fig. 11. The shear and elastic moduli increase with the content of glass powder. However, the increase is minor (less than 2%)

for 0% to 30% glass powder content, although the change is significant above 30% of glass powder (Figs. 11b-11d).

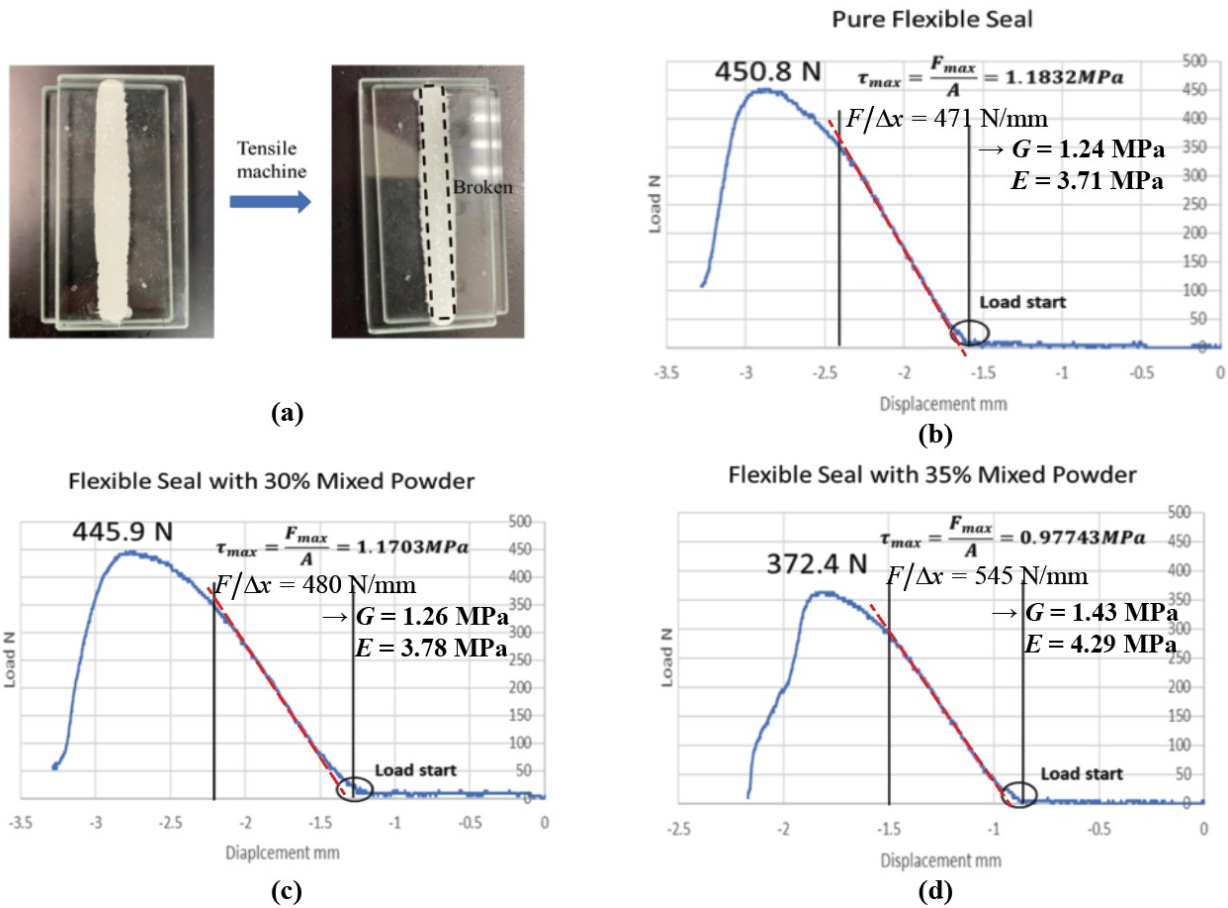


Figure 11. (a) A sample of glass with flexible seal for shear stress test using tensile testing machine. Shear stress test results for glass with three different seals: (b) pure flexible seal, (c) flexible seal mixed with 30% glass powder, and (d) flexible seal mixed with 35% glass powder.

3.3 Effect of Primary Seal Elastic Modulus on the Mechanical Response

Thermo-mechanical simulations were carried out using the quarter-window model as described earlier, in order to determine the displacement and stress fields for various components of the VIG under combined mechanical and thermal loads. The temperature difference between the outdoor and indoor environment causes the glass panes to have out-of-plane displacement, which is maximum at the center of the window, but still within the acceptable limit [15]. Stress values were examined at various locations of interest within the glass panes and the pillars [15], and also within the primary and secondary seals.

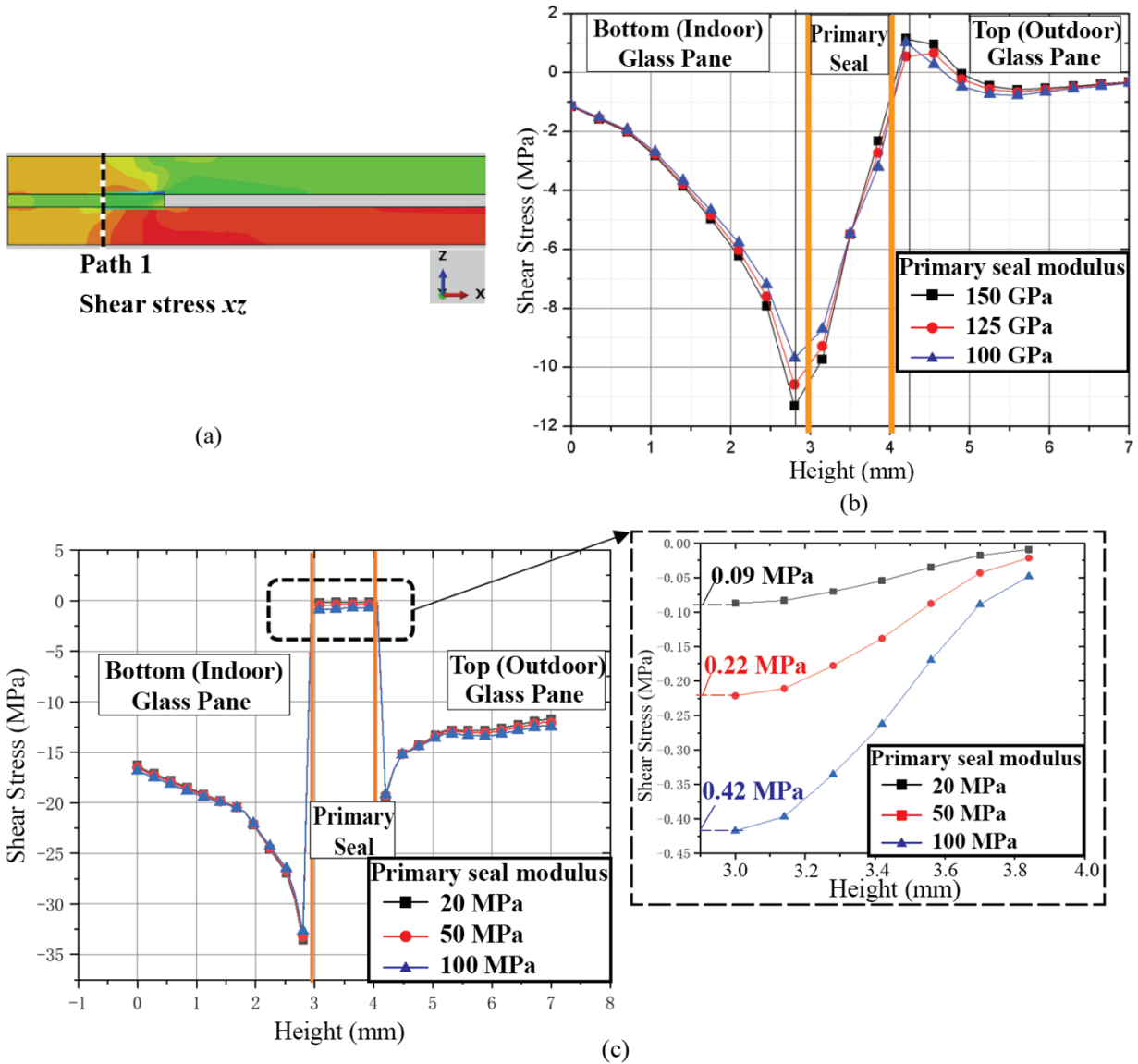


Figure 12. (a) Path for shear stress measurement, (b) xz component of the shear stress along a path that goes from the inside surface of the bottom glass pane to the outside surface of the top glass pane through the primary seal for different primary seal elastic modulus values between 100 – 150 GPa and (c) those between 20 – 100 MPa.

Simulations were carried out using different values for the elastic modulus of the primary seal. Values typical for the seal material used in conventional VIG units were considered initially, in the range of 100 – 150 GPa. The resulting plot of the shear stress along a path that goes from the inside surface of the bottom glass to the outside surface of the top glass is shown in Fig. 12a, with the xz component of the shear stress ranging from –12 to 1 MPa across the primary seal (Fig. 12b). It is observed that the maximum (negative)

shear stress becomes smaller with reduction in the elastic modulus of the primary seal.

In order to limit the shear stress in the primary seal, it was decided to use a flexible seal material as discussed above, with a modulus value that is considerably lower than conventional seal materials. The simulations were repeated with the primary seal elastic modulus varying between 20 – 100 MPa, with the corresponding results shown in Fig. 12c. The maximum shear stress values across the primary seal for different moduli range from 0.09 – 0.42 MPa, and these results are 2–10 times smaller than the maximum shear strength of the flexible seal from our experimental measurements (see Fig. 11). Moreover, the measured elastic moduli of flexible seals (Fig. 11) were lower than 5 MPa, which leads to a lower maximum stress than the values shown in Fig. 12. Therefore, it can be deduced that the flexible seal developed during this research is stable enough to maintain adequate vacuum conditions even in a 1 m × 1 m working VIG system.

4 Conclusions

The effects of edge-seal design on the mechanical strength and thermal insulation of VIG were studied using FEM simulations and experimental tests, including airtightness test and shear stress test. Through this research, the influence of the seal thermal conductivity and elastic modulus were evaluated for effective performance and optimal design of VIG, and flexible ceramic sealants were developed and tested for the VIG application.

The thermal insulation performance of VIG was evaluated using FEM simulations under different seal and pillar thermal conductivity values to study the influence of the seal on the thermal transport. Based on the analysis of FEM results, it was found that a lower seal conductivity k_{seal} results in a lower U -value of the VIG system. The extent of this influence depends on the range of k_{seal} ; for $k_{seal} > 1$ W/m.K, the influence in lowering the U -value is less significant, with only 5% difference in U -value from $k_{seal} = 1$ W/m.K to $k_{seal} = 10$ W/m.K. The heat flux distribution indicated that the region affected by the seal can extend to about three times the width of seal, and that when $k_{seal} < 1$ W/m.K, the impact on lowering the U -value is much greater. The results also indicate that the pillar conductivity k_{pa} does not have a significant influence on the sealing

effect.

A comparison between 3D and 2D simulations showed the importance of including the effect from the corner of the VIG unit in the calculation of overall thermal transmittance. Since the commonly used 2D simulations cannot account for the corner effect, they underestimate the U -value of the VIG. The higher temperatures at the corner can lead to higher stress variations, and therefore, special care should be taken while designing the corner construction of the the VIG for long term durability.

The flexible seal with different ratios of fine glass powder was tested in our experiments. When the volume fraction of the glass powder in the flexible seal was below 30%, it performed very well during the test, with no water leakage. However, when the ratio was larger than 40%, the seal material would lose most of its fluidity and could not be used to adequately bond and seal the glass panes. In addition, the higher volume fractions of glass powder also led to considerable deterioration of the shear strength. Comparisons with FEM simulation results showed that the measured shear strength values for the seal with < 30% glass powder were more than 10 times larger than the calculated shear stress values, which provides confidence in the ability of the flexible seal developed in this work to withstand the thermal and mechanical loads, and maintain adequate vacuum conditions during service, even in a 1 m × 1 m working VIG system.

CRedit author statement

Wenyuan Zhu: Methodology, Software, Validation, Formal analysis, Investigation, Data Curation, Writing - Original Draft, Visualization. **Bipin Shah:** Conceptualization, Software, Validation, Investigation, Writing - Review & Editing. **Sarma Gorti:** Methodology, Software, Investigation, Data Curation, Writing - Original Draft, Writing - Review & Editing. **Mahabir Bhandari:** Conceptualization, Investigation, Funding acquisition, Writing - Review & Editing, Project administration, Supervision. **Adrian Sabau:** Methodology, Software, Writing - Review & Editing. **Seungha Shin:** Data Curation, Investigation, Writing - Original Draft, Writing - Review & Editing, Supervision.

Acknowledgments

The authors greatly appreciate a financial support from the Buildings Technology Office of the US Department of Energy for this work. The authors specifically thank Marc LaFrance at the US Department of Energy for guiding this research. This work used the resources of the Extreme Science and Engineering Discovery Environment (XSEDE), which is supported by National Science Foundation grant number ACI-1053575.

References

1. R. E. Collins, G. M. Turner, A. C. Fischer-Cripps, J.-Z. Tang, T. M. Simko, C. J. Dey, D. A. Clugston, Q.-C. Zhang, and J. D. Garrison, "Vacuum glazing—a new component for insulating windows", *Building and Environment*, 1995. 30(4): p. 459-492.
2. *Review of Cost Effectiveness Analysis*. ENERGY STAR for Windows, Doors, and Skylights Version 6.0 Criteria Revision.
3. S. Grynning, A. Gustavsen, B. Time, and B. P. Jelle, "Windows in the buildings of tomorrow: Energy losers or energy gainers?", *Energy and Buildings*, 2013. 61: p. 185-192.
4. D. K. Benson, L. K. Smith, C. E. Tracy, T. Potter, C. Christensen, and D. E. Soule, "Vacuum window glazings for energy-efficient buildings: summary report" 1990, Internal Report SERI/TP-212-3684, Solar Energy Research Inst., Golden, CO (USA).
5. E. Cuce and P. M. Cuce, "Vacuum glazing for highly insulating windows: Recent developments and future prospects," *Renewable and Sustainable Energy Reviews*, 2016. 54: p. 1345-1357.
6. M. Rabani, H. B. Madessa, M. Ljungström, L. Aamodt, S. Løvvold, and N. Nord, "Life cycle analysis of GHG emissions from the building retrofitting: The case of a Norwegian office building", *Building and Environment*, 2021. 204(15): 108159.
7. S. J. Robinson and R. E. Collins, Evacuated windows-theory and practice, in ISES Solar World Congress (ISES, Kobe, Japan, 4-8 September 1989), pp. 1079-1083.

8. F. Zoller, Hollow pane of glass. German patent, 1924. 387655.
9. E. Cuce, C.-H. Young, and S. B. Riffat, "Thermal performance investigation of heat insulation solar glass: a comparative experimental study" *Energy and Buildings*, 2015. 86: p. 595-600.
10. M. M. Koebel, N. El Hawi, J. Lu, F. Gattiker, and J. Neuenschwander, "Anodic bonding of activated tin solder alloys in the liquid state: a novel large-area hermetic glass sealing method" *Solar Energy Materials and Solar Cells*, 2011. 95(11): p. 3001-3008.
11. S. L. Aggar, and V.S. Veerasamy, Vacuum IG unit with spacer/pillar getter. 2002, Google Patents.
12. M. Bao, X. Liu, J. Yang, and Y. Bao, "Novel hybrid vacuum/triple glazing units with pressure equalisation design" *Construction and Building Materials*, 2014. 73: p. 645-651.
13. Q. Zhu, W. Wu, Y. Yang, Z. Han, and Y. Bao, "Finite element analysis of heat transfer performance of vacuum glazing with low-emittance coatings by using ANSYS" *Energy and Buildings*, 2020. 206: p. 109584.
14. C. Kocer, "The thermal and mechanical performance of a vacuum insulating glazing" *Glass Performance Days*, 2015. June 24-26, 2015. Glaston, Finland.
15. W. Zhu, S. Zhang, S. Shin, S. Gorti, B. Shah, P. Joshi, and M. Bhandari, "Effects of pillar design on the thermal performance of vacuum-insulated glazing" *Construction and Building Materials*, 2022. 316: p. 125724.
16. I. Kowalczyk, D. Kozanecki, S. Krason, and M. Rabenda, "Computational modelling of VIG plates using FEM: Static and dynamic analysis," *Materials*, 2022. 15(4): p. 1467.
17. J. Park, M. Oh, and C. S. Lee, "Thermal performance optimization and experimental evaluation of vacuum-glazed windows manufactured via the in-vacuum method," *Energies*, 2019. 12(19): p. 3634.
18. Y. J. Shi, X. B. Xi, Y. F. Zhang, H. Y. Xu, J. F. Zhang, and R. H. Zhang, "Prediction and analysis of the thermal performance of composite vacuum glazing," *Energies*, 2021. 14(18): p. 5769.
19. S. Van Den Bergh, R. Hartd, B. P. Jelle, and A. Gustavsen, "Window spacers and edge seals in insulating glass units: A state-of-the art review and future perspectives" *Energy and Buildings*, 2013. 58: p. 263-280.

20. H. Jarimi, Q. Lv, O. Ramadan, S. Zhang, and S. Riffat, "Design, mathematical modelling and experimental investigation of vacuum insulated semi-transparent thin-film photovoltaic (PV) glazing" *Journal of Building Engineering*, 2020. 31: p. 101430.
21. Y. Fang, T. J. Hyde, F. Arya, N. Hewitt, P. C. Eames, B. Norton, and S. Miller, "Indium alloy-sealed vacuum glazing development and context" *Renewable and Sustainable Energy Reviews*, 2014. 37: pp. 480-501.
22. S. Memon, Y. P. Fang, and P. C. Eames, "The influence of low-temperature surface induction on evacuation, pump-out hole sealing and thermal performance of composite edge sealed vacuum insulated glazing," *Renewable Energy*, 2019. 135: p. 450-464.
23. S. Memon, and P.C. Eames, "Design and development of lead-free glass-metallic vacuum materials for the construction and thermal performance of smart fusion edge-sealed vacuum glazing" *Energy and Buildings*, 2020. 227: p. 110430.
24. ABAQUS 3DEXPERIENCE R2017x, Dassault Systemes SIMULIA Corp., Johnston, RI, 2017.
25. ASTM E2188-19, Standard Test Method for Insulating Glass Unit Performance, ASTM International: West Conshohocken, PA, 2019.
26. ASTM E2190-19, Standard Specification for Insulating Glass Unit Performance and Evaluation, ASTM International: West Conshohocken, PA, 2019.
27. ASTM C1199-14, Standard Test Method for Measuring the Steady-State Thermal Transmittance of Fenestration Systems Using Hot Box Methods. ASTM International: West Conshohocken, PA, 2014.
28. ASTM C518, Standard Test Method for Steady-State Thermal Transmission Properties by Means of the Heat Flow Meter Apparatus. ASTM International: West Conshohocken, PA, 2017.
29. R. C. Kerschbaumer, S. Stieger, M. Gschwandl, T. Hutterer, M. Fasching, B. Lechner, L. Meinhart, J. Hildenbrandt, B. Schritteser, P. F. Fuchs, G. R. Berger, and W. Friesenbichler, "Comparison of steady-state and transient thermal conductivity testing methods using different industrial rubber compounds" *Polymer Testing*, 2019. 80: p. 106121.

30. S.V. Charlie Curcija, R. Hart, J. Jonsson, R. Powles, and R. Mitchell, *WINDOW Technical Documentation*. 2018: Windows and Envelope Materials Group, Lawrence Berkeley National Laboratory Berkeley, California 94720.
31. THERM 7 / WINDOW 7 NFRC Simulation Manual, National Fenestration Rating Council, Inc. 2017.